

# Physics-guided Noise Neural Proxy for Low-light Raw Image Denoising

Hansen Feng, Lizhi Wang, *Member, IEEE*, Yiqi Huang, Yuzhi Wang,  
and Hua Huang, *Senior Member, IEEE*

**Abstract**—Low-light raw image denoising plays a crucial role in mobile photography, and learning-based methods have become the mainstream approach. Training the learning-based methods with synthetic data emerges as an efficient and practical alternative to paired real data. However, the quality of synthetic data is inherently limited by the low accuracy of the noise model, which decreases the performance of low-light raw image denoising. In this paper, we develop a novel framework for accurate noise modeling that learns a physics-guided noise neural proxy (PNNP) from dark frames. PNNP integrates three efficient techniques: physics-guided noise decoupling (PND), physics-guided proxy model (PPM), and differentiable distribution-oriented loss (DDL). The PND decouples the dark frame into different components and handles different levels of noise in a flexible manner, which reduces the complexity of the noise neural proxy. The PPM incorporates physical priors to effectively constrain the generated noise, which promotes the accuracy of the noise neural proxy. The DDL provides explicit and reliable supervision for noise modeling, which promotes the precision of the noise neural proxy. Extensive experiments on public low-light raw image denoising datasets and real low-light imaging scenarios demonstrate the superior performance of our PNNP framework.

**Index Terms**—Low-light Denoising, Noise Modeling, Neural Proxy, Computational Photography.

## 1 INTRODUCTION

WITH the increasing prevalence of cameras in mobile phones, it has become essential to deliver high-quality photography experiences, especially in low-light conditions. The inevitable noise in low-light conditions can lead to significant information loss, causing low-light raw image denoising a critical task. Learning-based denoising methods [1], [2], [3], [4], [5], [6], [7], [8], [9], *i.e.*, learning the noisy-to-clean mapping via the neural network, have become the mainstream approaches for low-light denoising, as they can learn data priors from massive data to compensate for the missing information. However, collecting a large-scale high-quality denoising dataset is a time-consuming and laborious process, which requires careful calibration of specialized equipment to ensure quality [10], [11], [12], [13], [14], [15], [16]. Therefore, training with synthetic data based on a noise model is an efficient and practical alternative [13], [14], [17], [18], [19].

Noise modeling aims to proxy the sensor noise for convenient resampling or reuse in subsequent stages. Physics-based noise modeling, as a classical and well-established approach, encompasses the modeling of noise by considering the underlying physical mechanisms and statistical properties of the sensor. For noise with known physical mechanisms, physics-based noise modeling provides accurate and interpretable noise representations, such as signal-dependent shot noise that can be equivalently modeled as Poisson noise. However, for noise with only partially known

physical mechanisms, hand-calibrated noise models often differ from the real noise model. There is still no consensus on a universal noise model for signal-independent read noise [20], [21], [22], [23]. To fill this gap, SFRN [19] samples real dark frames as signal-independent noise with corresponding post-processing methods. However, sampling cannot cover the entire range of continuous camera settings and diverse noise samples. In summary, the primary challenge of physics-based noise modeling lies in accurately representing the dominant component of noise (*i.e.*, read noise) under low-light conditions.

Learning-based noise modeling [24], [25], [26], [27], [28] has emerged as another prominent noise modeling approach in recent years. Learning-based noise modeling typically involves learning the clean-to-noise mapping via neural networks from paired real data. Leveraging high-quality paired real data, learning-based noise modeling can approximate the real noise model even when the physical mechanisms of the sensor are not fully known. However, obtaining high-quality paired real data is challenging and data quality hinders the accurate neural proxy of the noise model, rendering learning-based noise modeling methods ineffective in practical scenarios [14], [19]. First, due to underdeveloped data acquisition settings and inevitable environmental disturbances, paired real data typically suffer from spatial and intensity misalignment. As a result, neural networks may mistakenly interpret these misalignments as noise to be modeled. Second, due to the coupling of excessive noise models within the paired real data, the clean-to-noise mapping becomes complex and the noise distribution is difficult to measure. As a result, neural networks often converge unstably and finally reach suboptimal solutions. In summary, the primary challenges of learning-based noise modeling lie in the reliance on high-quality paired real data

- Hansen Feng, Lizhi Wang and Yiqi Huang are with the School of Computer Science and Technology, Beijing Institute of Technology, Beijing, 100081, China. Email: {fenghansen, wanglizhi, huangyiqi}@bit.edu.cn
- Yuzhi Wang is with the Megvii Technology, Beijing, 100086, China. Email: justin.w.xd@gmail.com
- Hua Huang is with the School of Artificial Intelligence, Beijing Normal University, Beijing, 100875, China. Email: huahuang@bnu.edu.cn

and the associated issues related to data quality.

We observe that physics-based noise modeling and learning-based noise modeling are complementary to each other. Therefore, we propose a novel strategy for noise modeling, which involves learning noise neural proxy from dark frames instead of paired real data. From the perspective of physics-based noise modeling, employing neural networks to represent dark frames containing read noise can further promote the accuracy of noise modeling. From the perspective of learning-based noise modeling, dark frames are easier to collect compared to paired real data and are no longer influenced by signal misalignment presented in paired real data.

To further exploit the opportunities brought by the strategy, we introduce a physics-guided noise neural proxy (PNNP) framework. The noise model within dark frames is still complex, making the precise measurement and approximation of the noise model challenging. Our framework leverages the physical priors of the sensor to decouple the complex noise, constrain the optimization process, and provide reliable supervision, thereby further improving the performance of noise neural proxy.

Firstly, we propose a physics-guided noise decoupling (PND) to handle different levels of noise in a flexible manner. Based on the statistical properties of noise, we decouple the dark frame into frame-wise, band-wise, and pixel-wise components. We model the frame-wise and band-wise noise via physics-based noise calibration methods while employing a neural network to proxy the pixel-wise noise only. Our noise decoupling strategy simplifies the complexity of the noise neural proxies, thereby reducing the complexity of the noise neural proxy.

Moreover, we propose a physics-guided proxy model (PPM) incorporating physical priors to constrain the generated noise. Referring to the imaging process of sensors, we propose an interpretable network architecture to achieve physical constraints. Our proxy model restricts the degrees of freedom during optimization based on physical priors, thereby promoting the accuracy of noise neural proxy.

Finally, we propose a differentiable distribution-oriented loss (DDL) to efficiently supervise the random noise variables. Leveraging the cumulative distribution function (CDF) as a foundation, we propose a quantile loss function and a CDF loss function with their corresponding training strategies. Our loss function provides explicit and reliable supervision for noise modeling, thereby promoting the precision of noise neural proxy.

The effective integration of physics-based and learning-based noise modeling is the core competitiveness of our framework. Our framework introduces statistical constraints into neural proxies based on physical priors, while also learning the continuous representation of real sensor noise through neural proxies. Extensive experiments on public low-light raw image denoising datasets [12], [13], [14] and real low-light imaging scenarios demonstrate the superior performance of our framework compared to existing noise modeling methods.

In summary, our main contributions can be summarized as follows:

- 1) We introduce the strategy of learning noise neural proxy from dark frames instead of paired real data, and

then propose the physics-guided noise neural proxy framework to effectively integrate the physics-based and learning-based noise modeling.

- 2) We propose a physics-guided noise decoupling to enable the neural network to approximate pixel-wise noise only, which reduces the complexity of noise neural proxy.
- 3) We propose a physics-guided proxy model to ensure that the synthesized noise adheres to the physical priors, which promotes the accuracy of noise neural proxy.
- 4) We introduce a differentiable distribution-oriented loss to provide explicit and reliable supervision, which promotes the precision of noise neural proxy.

## 2 RELATED WORKS

### 2.1 Low-light Raw Image Denoising

Due to the inherent advantages of raw images characterized by high bit depth and high linearity, low-light raw image denoising has garnered significant attention in the industry and has been subject to extensive research in various fields, including astronomy [29], microscopy [30] and mobile photography [31].

Classical denoising methods relying on image priors such as sparsity [32], [33], low rank [34], self-similarity [35], [36], and smoothness [37], [38], can generally be applied to low-light raw image denoising. However, the effectiveness of image priors is ultimately limited in low-light conditions, making it challenging to achieve satisfactory denoising results for the corrupted images. With the development of deep learning, learning-based methods [12], [39], [40] have emerged as the mainstream approach for low-light raw image denoising.

Training a neural network requires large-scale high-quality data, which is a significant challenge in low-light raw image denoising. On one hand, the extreme imaging settings increase the difficulty of data collection. The combination of complex physical environments and challenging imaging settings typically results in underdeveloped datasets, characterized by either insufficient quantity or compromised quality. On the other hand, the extreme imaging settings amplify errors in the noise model. The classical heteroscedastic Gaussian noise model [41] fails to generate reliable training data, highlighting the indispensability of research on noise modeling in practice.

Recently, PMN [42] integrate paired real data and noise modeling based on the concept of learnability enhancement. Inspired by the PMN, we revisit existing noise modeling methods from a data perspective and finally achieve comparable or even superior denoising performance.

### 2.2 Noise Modeling

Noise modeling aims to proxy the sensor noise for convenient resampling or reusing in image processing. Based on the correlation of signals, sensor noise is typically divided into “shot noise” and “read noise”. In raw image denoising, the most classic noise modeling approach is the Poisson-Gaussian model or simplified heteroscedastic Gaussian model [41]. The noise model parameters are often specific to the sensors, thus requiring noise calibration for

specific cameras [20], [41], [43]. The calibrated noise parameters can also serve as noise priors for certain Variance-Stabilizing Transformation (VST) methods [18], [44], [45], [46], thereby further enhancing denoising performance.

However, classical noise modeling approaches tend to be limited in low-light conditions. Shot noise modeling, based on the photoelectric effect, is relatively reliable due to well-defined physical processes. In contrast, the origin of read noise is highly complex, and there is no consensus on its noise model in the imaging community [20], [22], [23], [47], [48], [49]. In response to this challenge, there are several noise modeling works specifically targeting low-light conditions in recent years. [13], [14] propose a physics-based noise modeling method for extreme low-light photography, improving the accuracy of noise modeling in low-light conditions. [19] propose to directly sample from dark frames and perform high-bit recovery to synthesize noisy data, trading off noise accuracy for data diversity. [42] introduce a linear dark shading model and a shot noise augmentation method, opening up a new perspective on the relationship between paired real data and noise modeling.

In recent years, there has been a surge in learning-based noise modeling methods. Learning-based noise modeling can incorporate statistical constraints from physical priors and learn continuous representations from real samples. However, the use of imprecise distribution measure methods has often limited the effectiveness of learning-based noise modeling compared to physics-based approaches. For instance, [24] and [28] employ normalized flows to transform Gaussian noise into real noise. Nevertheless, their frameworks struggle to capture complex noise patterns in low-light conditions. Similarly, noise modeling methods based on Generative Adversarial Networks (GANs) [25], [26], [27], [50] face challenges in effectively measuring noise models, relying heavily on the good initialization provided by physics-based noise modeling for optimal performance.

We have identified various signal-wise defects in the existing paired real data present in denoising datasets, including noise residues, spatial misalignment and brightness inconsistency. Existing learning-based noise modeling methods tend to overlook or incorporate these defects as part of the noise, resulting in overfitting to the training scene and underfitting to the noise model. Addressing the issue of data quality and enabling reliable measurements both serve as the foundation of our work.

### 3 METHOD

In this section, we first introduce the strategy and framework of physics-guided noise neural proxy (PNNP). Then, we introduce the three efficient techniques, *i.e.*, physics-guided noise decoupling (PND), physics-guided proxy model (PPM), and differentiable distribution-orient loss (DDL), respectively.

#### 3.1 Strategy and Framework

In order to clearly introduce our strategy and framework of PNNP, we will first provide a brief overview of the general sensor imaging model.

During the sensor imaging process, the incident scene irradiance  $I$  undergoes several transformations, including

conversion to charges and subsequently voltages, amplification by amplifiers, and quantization into the digital signal  $D$  by an analog-to-digital converter (ADC) [20]. For a raw image captured by a sensor, the imaging model can be expressed as:

$$D = K(I + N_p) + N_{read}, \quad (1)$$

where  $K$  represents the overall system gain,  $N_p$  is the signal-dependent photon shot noise, and  $N_{read}$  is signal-independent read noise. The general noise model can be extracted as:

$$N = KN_p + N_{read}. \quad (2)$$

In the general noise model, the shot noise model based on the photoelectric effect is relatively reliable due to well-defined physical processes, which can be modeled as:

$$(I + N_p) \sim \mathcal{P}(I), \quad (3)$$

where  $\mathcal{P}$  denotes the Poisson distribution. In contrast, the origin of read noise is highly complex, and there is no consensus on its noise model in the imaging community [20], [22], [23], [47], [48], [49]. In low-light conditions, the contribution of read noise is much higher compared to that in normal light conditions, thus further emphasizing the need for accurate noise modeling.

Unfortunately, existing noise modeling strategies suffer from certain limitations. The physics-based noise modeling strategies involve decoupling the noise model and performing hand-calibrated modeling separately. However, due to sensor variations and unknown read noise, hand-calibrated noise models struggle to accurately represent the real noise model. The learning-based noise modeling strategies utilize powerful neural networks to learn proxy models from paired real data, leveraging their high representational capacity. However, the inherent quality issues present in paired real data prevent the neural networks from effectively approximating the real noise model. Therefore, a new strategy of noise modeling is required to address these challenges and fundamentally enhance noise modeling techniques.

In this paper, we propose a novel strategy that integrates both physics-based and learning-based noise modeling by learning the noise model from dark frames instead of paired real data. The strategy addresses the limitations of representation in physics-based noise modeling through data-driven proxy models, as well as compensates for the data deficiency in learning-based noise modeling through physics-guided noise decoupling.

Motivated by this new strategy, we introduce a novel noise modeling framework called the PNNP framework, as shown in Fig. 1. Firstly, we propose a physics-guided noise decoupling. We decouple dark frames into three independent levels: frame-wise, band-wise, and pixel-wise. Dark frames contain the complete read noise, hence we rewrite Eq. (1) as:

$$D = K(I + N_p) + N_{frame} + N_{band} + N_{pixel}, \quad (4)$$

where  $N_{frame}$  represents the temporal stable frame-wise noise,  $N_{band}$  represents the row- or col-related band-wise noise, and  $N_{pixel}$  represents the independent and identically distributed (i.i.d.) pixel-wise noise.

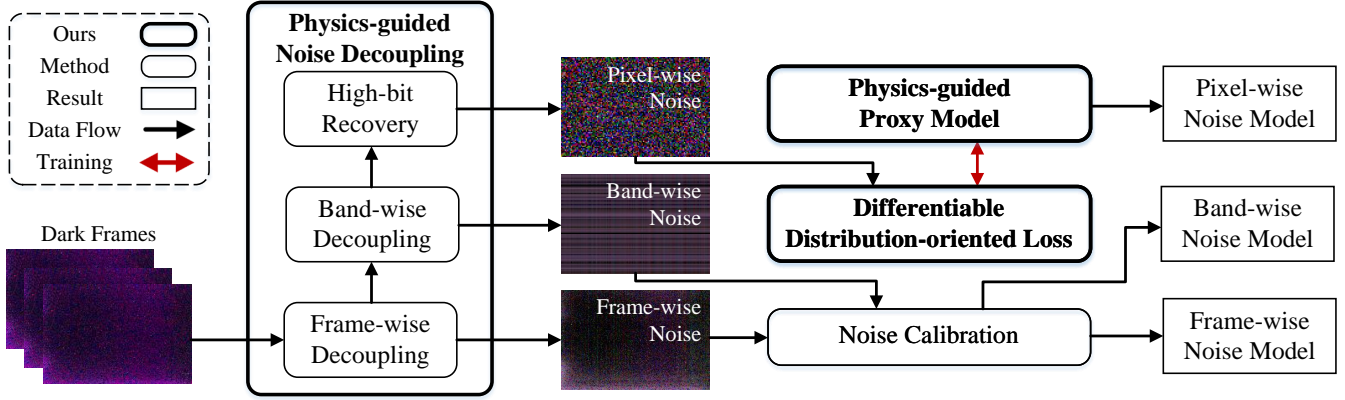


Fig. 1. The overview of our physics-guided noise neural proxy (PNNP) framework.

Within the proposed framework, we leverage the frame-wise noise and band-wise noise to calibrate their respective noise models using established physics-based noise calibration methods [13], [14], [42]. Notably, our primary focus lies in accurately modeling the pixel-wise noise, a challenging task for previous physics-based noise modeling methods. Therefore, we employ a powerful neural network as the proxy model of pixel-wise noise. The decoupled pixel-wise noise exhibits the favorable characteristic of spatial independence, which serves as a valuable physical prior. To fully exploit the physical prior, we introduce the PPM to represent the pixel-wise noise and utilize the DDL to measure the distribution distance. Through precise and efficient training, we are able to obtain the pixel-wise noise model. Detailed implementation specifics of the PND, PPM, and DDL will be elaborated in subsequent sections of the paper.

In summary, the PNNP framework simplifies the complexity of noise neural proxies, combining the advantages of physics-based and learning-based approaches to enhance the accuracy of noise modeling.

### 3.2 Physics-guided Noise Decoupling

In this section, we will introduce the principles and procedures of physics-guided noise decoupling in detail.

Previous research [42] has highlighted the advantages of noise decoupling in reducing data mapping complexity and improving denoising performance. We extend this notion to noise modeling, demonstrating that noise decoupling offers advantages beyond denoising. By employing different modeling approaches to address distinct levels of noise, we can effectively reduce the complexity associated with noise neural proxies. In line with the physical mechanisms and statistical characteristics of noise, we decouple dark frames into three distinct noise types with significant mode differences: frame-wise noise, band-wise noise, and pixel-wise noise. The decoupling process of a dark frame is illustrated in Fig. 2.

Initially, the original dark frame, captured in a lightless environment, is represented as a discrete signal with quantization intervals. In the decoupling process, we first employ frame-wise decoupling to remove the temporally stable frame-wise noise. As a result, the dark frame devoid of

frame-wise noise no longer exhibits significant spatial non-uniformity and retains various random noise components. Subsequently, we employ band-wise decoupling to eliminate the statistically patterned band-wise noise, resulting in a dark frame with reduced spatial correlation, where only i.i.d. pixel-wise noise remains. Due to the low-bit quantization of the original dark frame, the noise distribution of the pixel-wise noise exhibits periodic fluctuations caused by quantization-induced signal misalignment, as shown in Fig. 2. To mitigate the impact of quantization-induced signal misalignment on the noise neural proxy, we perform high-bit reconstruction [19] to eliminate the influence of quantization noise. The resulting high-bit pixel-wise noise serves as the ground truth for subsequent noise neural proxy modeling. The observed significant variations in noise distribution and noise intensity (standard deviation) in Fig. 2 indicate the effectiveness of our physics-guided noise decoupling.

Next, we introduce the principles and procedures of frame-wise decoupling, band-wise decoupling, and high-bit reconstruction, respectively.

Frame-wise noise, also known as dark shading [49], represents the temporal stable component of read noise and encompasses both spatial invariant Black Level Error (BLE) [14], [51] and spatial variant Fixed Pattern Noise (FPN) [20], [21], [23], [48], [52]. Following previous works [28], [42], we first compute the average of dark frames at the same ISO to estimate the ISO-specific frame-wise noise. Then, we utilize a linear dark shading model to fit the ISO-specific frame-wise noise at different ISO as the final frame-wise noise model

$$N_{frame} = N_{FPNk} \cdot iso + N_{FPNb} + BLE(iso), \quad (5)$$

where  $N_{FPNk} \in \mathbb{R}^{H \times W}$  and  $N_{FPNb} \in \mathbb{R}^{H \times W}$  are the coefficient maps of the FPN that needs to be regressed,  $iso$  is the ISO value,  $BLE(iso)$  is the BLE at a specific ISO value  $iso$ .

It is worth noting that the frame-wise noise used for denoising is reconstructed from the frame-wise noise model instead of the ISO-specific frame-wise noise. This choice offers two main advantages. Firstly, estimating the linear dark shading model leverages more dark frames across different ISO levels, thereby reducing the influence of random noise. Secondly, parameterizing the linear dark shading

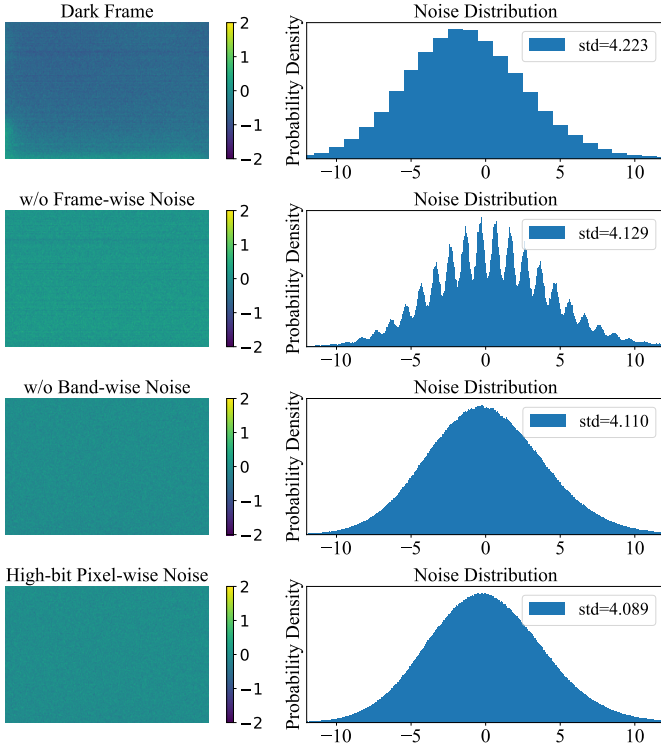


Fig. 2. The demonstration of the PND. The first and second columns plot the noise and its corresponding noise distribution, respectively. The numerical range has been adjusted for better visualization. “std” refers to the standard deviation of the noise, which characterizes the intensity of the noise.

model allows us to introduce small perturbations to each parameter during training to simulate calibration errors.

The band-wise noise can be primarily divided into row noise  $N_{row}$  and column noise  $N_{col}$ , which are typically associated with the working frequency and readout mechanism of the sensor circuit

$$N_{band} = N_{row} + N_{col}. \quad (6)$$

Following previous works [13], [14], we model the band-wise noise as zero-mean Gaussian noise

$$N_{row} \sim \mathcal{N}(0, \sigma_{row}^2), N_{col} \sim \mathcal{N}(0, \sigma_{col}^2), \quad (7)$$

where  $N_{row} \in \mathbb{R}^{H \times 1}$  and  $N_{col} \in \mathbb{R}^{1 \times W}$ .

The band-wise noise can be easily estimated by computing the mean of each row or column in the dark frames. The goodness of fit can be evaluated using the coefficient of determination in the probability plot, denoted as  $R^2$  [53]. In our experiments, the  $R^2$  for fitting the band-wise noise with a Gaussian distribution exceeds 0.999, indicating a strong adherence of the band-wise noise to the assumption of a Gaussian distribution.

After the aforementioned physics-guided noise decoupling, the remaining noise corresponds to the pixel-wise noise, which can be considered as the aggregation of all i.i.d. noise within the sensor. As introduced at the beginning of this section, the pixel-wise noise obtained from the noise decoupling exhibits quantization-induced signal misalignment. Therefore, we employ the high-bit reconstruction

technique proposed in SFRN [19] to reconstruct the pixel-wise noise. It is worth noting that SFRN does not perform noise decoupling to high-bit reconstruction, resulting in non-i.i.d. signals that affect the accuracy of high-bit reconstruction. The effectiveness of the high-bit reconstruction technique relies on our noise decoupling strategy, which is not considered in existing works.

In summary, the physics-guided noise decoupling strategy simplifies the complexity of the noise neural proxies, thereby reducing the complexity of the noise neural proxy.

### 3.3 Physics-guided Proxy Model

As shown in Fig. 3, we propose the PPM to adapt the data flow of the new strategy. Our overall network architecture adopts a lightweight dual-branch cylindrical design. The input to PPM is the random noise  $N_z$  that follows a standard normal distribution. We divide the input into two parts,  $z_{pre}$  and  $z_{fol}$ , which are separately fed into the ISO-dependent branch and the ISO-independent branch. The two branches of the network share identical structures, which include  $1 \times 1$  convolutions, Swish activation functions, and residual blocks composed of these operations. Following the physical imaging process of reference sensors, the output  $y_{pre}$  from the ISO-dependent branch undergoes amplification using a gain layer  $g(ISO)$ , while the output  $y_{fol}$  from the ISO-independent branch remains unchanged regardless of ISO variations. The sum of the outputs from these dual branches, denoted as  $y_{out}$ , represents the noise transformation result of our proxy model. To optimize the model, the final output  $y_{out}$  is supervised to approximate the ground truth noise  $y_{real}$  by using the quantile loss  $L_{quantile}$  and CDF loss  $L_{CDF}$ . The process can be summarized as follows:

$$N_{pixel} = \text{PPM}(N_z), \quad (8)$$

where pixel-wise noise  $N_{pixel} \in \mathbb{R}^{H \times W}$  and the random noise  $N_z \in \mathbb{R}^{2 \times H \times W}$ .

We provide a detailed explanation of the two physics-guided designs incorporated in our network.

Firstly, we introduce the design of the pixel-wise independent module. Considering the i.i.d. nature of pixel-wise noise, all module designs utilize spatially independent operations, employing  $1 \times 1$  convolutions instead of  $3 \times 3$  convolutions. Despite the theoretical advantage of  $3 \times 3$  convolutions in terms of optimization freedom, as  $3 \times 3$  convolutions encompass the search space of  $1 \times 1$  convolutions,  $3 \times 3$  convolutions can pose an optimization trap in practical scenarios. The presence of non-zero parameters in  $3 \times 3$  convolutions (except the central parameter) introduces spatial correlation, which contradicts the prior assumption of pixel-wise spatial independence. Therefore, when dealing with pixel-wise noise, the use of  $1 \times 1$  convolutions in the proxy model becomes crucial. By adhering to the structural constraint of  $1 \times 1$  convolutions, the proxy model significantly reduces its optimization freedom while adhering to the prior assumption of spatial independence.

Next, we introduce the design of the ISO-aware dual branch. The noise pattern is significantly affected by analog amplifiers in sensor circuits. Inspired by the physical principle of noise amplification in analog amplifiers, we divide the network into ISO-dependent and ISO-independent

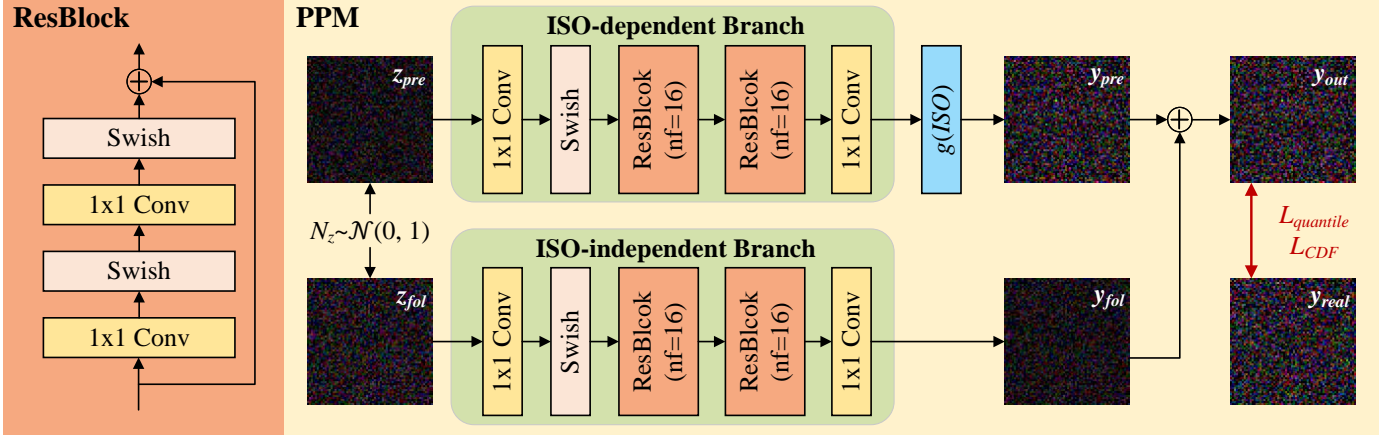


Fig. 3. The overview of our physics-guided proxy model (PPM).

branches. Typically, conventional sensor gains exhibit linear growth with ISO. Therefore, we design an ISO-dependent gain layer, denoted as  $g(ISO)$ , based on the linear gain prior, which is equivalent to the analog gain  $K$ . In this paper, we adopt the approach of directly modeling  $g(ISO)$  using parameters obtained from noise calibration, which contributes to convergence. By leveraging the explicit modeling of the ISO-aware dual branch network, the proxy model effectively bridges the noise model across different ISO levels while maintaining interpretability.

In summary, the physics-guided proxy model restricts the degrees of freedom during optimization based on physical priors, thereby promoting the accuracy of noise neural proxy.

### 3.4 Differentiable Distribution-oriented Loss

The choice of loss function poses a major challenge in learning-based noise modeling, as it is difficult to accurately measure the distance between noise distributions based on a set of noise samples. Previous methods can only measure the distribution through indirect approaches to train neural networks. A common approach is to employ Generative Adversarial Networks (GANs) [54]. GANs employ neural networks to extract noise features and estimate the distance between these features, indirectly quantifying the distance between noise distributions. However, GANs are known to be prone to instability and overfitting, often requiring careful initialization for effective convergence in noise modeling. Another common approach is to employ normalizing flow-based methods [55]. The invertible neural network of the flow-based model is bijective. By learning the transformation process from unknown real noise to known Gaussian noise, the model can simultaneously acquire the reverse process, which corresponds to noise modeling. However, the strict reversibility also limits the performance of flow-based models, leading to the underfitting of the noise model.

Our noise decoupling strategy brings pixel-wise noise with spatial independence, which provides a new opportunity for designing loss functions in noise modeling. We observe that the distribution function of i.i.d. pixel-wise noise can serve as a representation of the noise model itself.

Motivated by this insight, we propose the DDL that leverages cumulative distribution functions (CDFs) for precise and interpretable measurements of the noise distribution. Instead of forcing complex data to fit measurement methods, we simplify the data to align with reliable measurement techniques.

Specifically, we introduce two distribution-oriented loss functions: quantile loss  $L_{quantile}$  and CDF loss  $L_{CDF}$ . Quantiles are values that divide a probability distribution into equal parts, while the CDF characterizes the probability of a random variable taking on a value less than or equal to a given value. As shown in Fig. 4(a), quantiles and CDF can be seen as the horizontal and vertical axes, respectively, of a distribution function plot. They represent the coordinates of points on the distribution curve. Hence, the distance between two points on the distributions can be measured by the difference between their corresponding quantiles and CDF values, which forms the foundation for the quantile loss  $L_{quantile}$  and the CDF loss  $L_{CDF}$ .

To enable the training of neural networks using distribution-oriented loss functions, it is essential to ensure the differentiability of the loss computation process. Since noisy samples are discrete data, their CDF is obtained through sorting and normalization. Fortunately, the sorting and normalization operations preserve gradients, allowing us to make the querying process of quantiles and CDF differentiable, which ensures the overall differentiability of the loss computation process.

Taking CDF as an example, for a noisy sample set with a total of  $n$  samples, the CDF of the  $i$ -th smallest value, denoted as  $p_i$ , is given by  $F(i) = i/n$ . The query operation first employs binary search to find the smallest index  $i$  such that  $q_i$  is not less than a given value  $q$ . As shown in Fig. 4(b), the query result  $p$  is obtained by linear interpolation between the samples  $q_{i-1}$  and  $q_i$  surrounding the given value  $q$ :

$$p = F(q) = \left( i - \frac{q_i - q}{q_i - q_{i-1}} \right) / n, \quad (9)$$

where we augment the data with negative infinity and apply appropriate corrections to support arbitrary value queries.

All the operations involved in the above process are differentiable, ensuring the differentiability of the distribution-

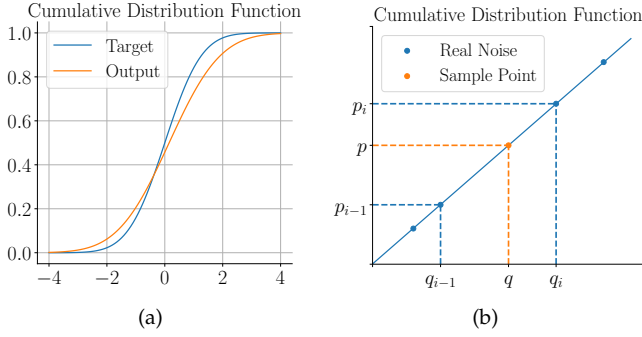


Fig. 4. The principle of DDL. (a) The cumulative distribution function plot, which is used to characterize the distribution distance between the target and the output. (b) The cumulative distribution function plot after partial zoom-in, which is used to demonstrate the linear interpolation in the query operation process.

oriented loss function. The derivation of the quantile loss follows a similar approach, which is omitted here for brevity.

Next, we provide the formal definitions of our quantile loss  $L_{quantile}$  and CDF loss  $L_{CDF}$ . For arbitrary pixel-wise noise  $y$ , its CDF is denoted as  $F$ , and its quantile function is denoted as  $F^{-1}$ . Given two pixel-wise noise samples  $y_{out}$  and  $y_{real}$ , the set of query value sampling points is denoted as  $Q = \{q_k | k = 1, 2, \dots, N\}$ . The CDF loss  $L_{CDF}$  is defined as:

$$L_{CDF} = \sum_{k=1}^N |F_{out}(q_k) - F_{real}(q_k)|, \quad (10)$$

where  $F_{out}$  and  $F_{real}$  represent the CDFs of pixel-wise noise  $y_{out}$  and  $y_{real}$ , respectively.

Similarly, the quantile loss  $L_{quantile}$  is defined as:

$$L_{quantile} = \sum_{k=1}^N |F_{out}^{-1}(p_k) - F_{real}^{-1}(p_k)|, \quad (11)$$

where  $F_{out}^{-1}$  and  $F_{real}^{-1}$  represent the quantile functions of pixel-wise noise  $y_{out}$  and  $y_{real}$ , respectively.

Each query operation typically provides supervision for only two samples around the query value. Therefore, the sampling strategy for query values plays a crucial role in the efficiency of the loss function. We employ a random sampling strategy that introduces slight perturbations to fixed samples, enhancing the robustness of supervision. Initially, we use uniform sampling on the standard normal distribution as a baseline, covering the entire noise distribution in an uniform manner. Gaussian perturbations are then added around the baseline to increase the diversity of supervised points. We clip the query values to avoid numerical overflow. The DDL based on the random sampling strategy can effectively and accurately fit the noise.

In summary, the distribution-oriented loss function provides explicit and reliable supervision for the noise model, thereby promoting the precision of the noise neural proxy.

## 4 EXPERIMENT

In this section, we first introduce the experimental setting including the implementation details and the compared methods (Section 4.1). Then, we evaluate our method in

comparison to other existing methods on public datasets (Section 4.2). After that, we conduct comprehensive ablation studies to analyze our methods (Section 4.3). Finally, we evaluate the generalizability of our method on real imaging scenarios of a mobile phone (Section 4.4).

### 4.1 Experimental Setting

#### 4.1.1 Implementation details

**Noise Modeling.** The dark frames for noise modeling on the SID dataset [12] and ELD dataset [13], [14] are captured using a Sony A7S2 camera, which shares the same sensor as the public datasets but not the same camera. We prepare 10 dark frames per ISO for our physics-guided noise neural proxy framework. After physics-guided noise decoupling, we randomly crop  $1024 \times 1024$  patches at each step to train the PPM. We train the PPM with 1000 steps using Adam [56] and our DDL. We sample  $10^4$  query values per step according to our sampling strategy. The learning rate follows a variation pattern similar to SGDR [57]. The base learning rate is set to  $10^{-2}$  and the minimum learning rate is set to  $10^{-5}$ .

Inspired by previous works on noise modeling [13], [14], [51], we additionally record the calibration error of dark shading under the Gaussian error assumption. During noise synthesis, we introduce perturbation noise based on the recorded calibration errors, which can enhance the robustness of the denoising model. To simulate extreme FPN variations, we introduce a 10% probability of the FPN perturbation with a magnitude of ten times larger than the calibration error.

**Low-light Raw Image Denoising.** We employ the same UNet architecture [58] as ELD for denoising. We utilize raw images from the SID Sony training set following Eq.(4) to synthesize training data. The quantitative results are reported on the ELD Sony dataset and the whole SID Sony dataset, including validation and test sets. We adopt the dark shading correction strategy [42], thus we correct the frame-wise noise before inference. For training, we pack the raw Bayer images into four channels and sample non-overlapped  $512 \times 512$  patches from each image. These patches are then randomly rotated and flipped as a batch. We visualize the raw images as sRGB images for viewing through Rawpy (a Python wrapper for LibRaw) utilizing the metadata of ground truth following the previous works [12], [14]. The quantitative results are computed on the raw images.

We train denoising models for 1800 epochs using Adam optimizer and  $L_1$  loss. Each epoch consists of data pairs from various scenarios and exposure ratios. The learning rate will vary with iterations similar to SGDR. The base learning rate is set to  $2 \times 10^{-4}$  and the minimum learning rate is set to  $10^{-5}$ . The optimizer restarts every 600 epochs and the learning rate is halved on restarts.

**Compared methods.** In order to demonstrate the reliability of our PNNP framework, we compare our noise model with the following approaches:

- The denoising model trained with paired real data (*i.e.*, Paired Data), serves as a baseline for evaluating the performance of noise modeling applied to denoising.

TABLE 1

Quantitative results (PSNR/SSIM) of different methods on the ELD dataset and SID dataset. The red color indicates the best results and the blue color indicates the second-best results.

Method	Metrics	ELD [14]		SID [12]		
		×100	×200	×100	×250	×300
Paired Data	PSNR / SSIM	44.47 / 0.9676	41.97 / 0.9282	42.06 / 0.9548	39.60 / <b>0.9380</b>	36.85 / <b>0.9227</b>
NoiseFlow [24]	PSNR / SSIM	41.05 / 0.9249	39.23 / 0.8886	38.88 / 0.9287	35.80 / 0.8668	32.29 / 0.8009
CA-GAN [26]	PSNR / SSIM	41.48 / 0.9330	39.26 / 0.8771	38.66 / 0.9209	35.30 / 0.8463	32.02 / 0.7685
Starlight [27]	PSNR / SSIM	43.80 / 0.9358	40.86 / 0.8837	40.47 / 0.9261	36.26 / 0.8575	33.00 / 0.7802
LLD [28]	PSNR / SSIM	45.78 / 0.9789	44.08 / <b>0.9635</b>	42.29 / 0.9562	40.11 / 0.9373	36.89 / 0.9152
P-G [41]	PSNR / SSIM	42.05 / 0.8721	38.18 / 0.7827	39.44 / 0.8995	34.32 / 0.7681	30.66 / 0.6569
ELD [14]	PSNR / SSIM	45.45 / 0.9754	43.43 / 0.9544	41.95 / 0.9530	39.44 / 0.9307	36.36 / 0.9114
SFRN [19]	PSNR / SSIM	<b>46.38</b> / <b>0.9793</b>	<b>44.38</b> / <b>0.9651</b>	<b>42.81</b> / <b>0.9568</b>	<b>40.18</b> / 0.9343	<b>37.09</b> / 0.9175
PNNP (Ours)	PSNR / SSIM	<b>47.11</b> / <b>0.9835</b>	<b>44.89</b> / <b>0.9635</b>	<b>43.75</b> / <b>0.9580</b>	<b>41.38</b> / <b>0.9444</b>	<b>37.78</b> / <b>0.9243</b>

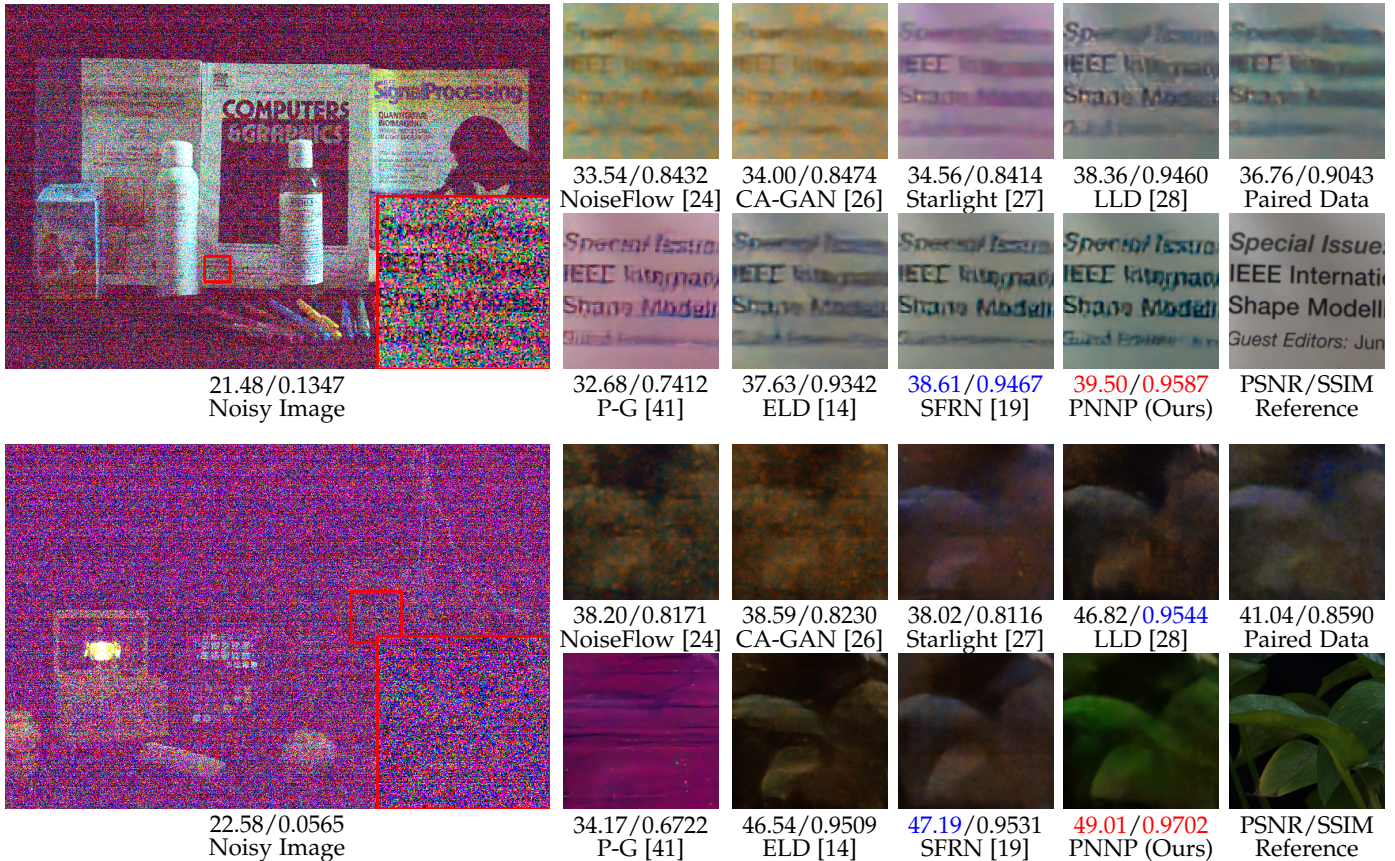


Fig. 5. Raw image denoising results on images from the ELD dataset. The red color indicates the best results and the blue color indicates the second-best results. (Best viewed with zoom-in)

- Learning-based noise modeling methods including Noise Flow [24], CA-GAN [26], starlight [27] and LLD [28].
- Physics-based noise modeling methods including Poisson-Gaussian (P-G) [41], ELD [14] and SFRN [19].

The results of learning-based noise modeling methods are provided by the previous work [28]. The results of P-G, ELD, and Paired Data are implemented from the code and weights released by the open-source project. Since the training code and weights of SFRN have never been released, we reproduce the SFRN with the help of the authors, and the results of the experiments have been confirmed by the

authors.

It is important to emphasize that our evaluation and comparison of noise modeling methods primarily focus on the performance of the noise models in denoising tasks. This decision stems from our observation that the conventional practice of employing distribution-oriented metrics to assess noise models is not well-suited to the existing datasets.

## 4.2 Denoising on Public Datasets

Table 1 summarizes the denoising performances over different exposure ratios of the denoising model trained with the

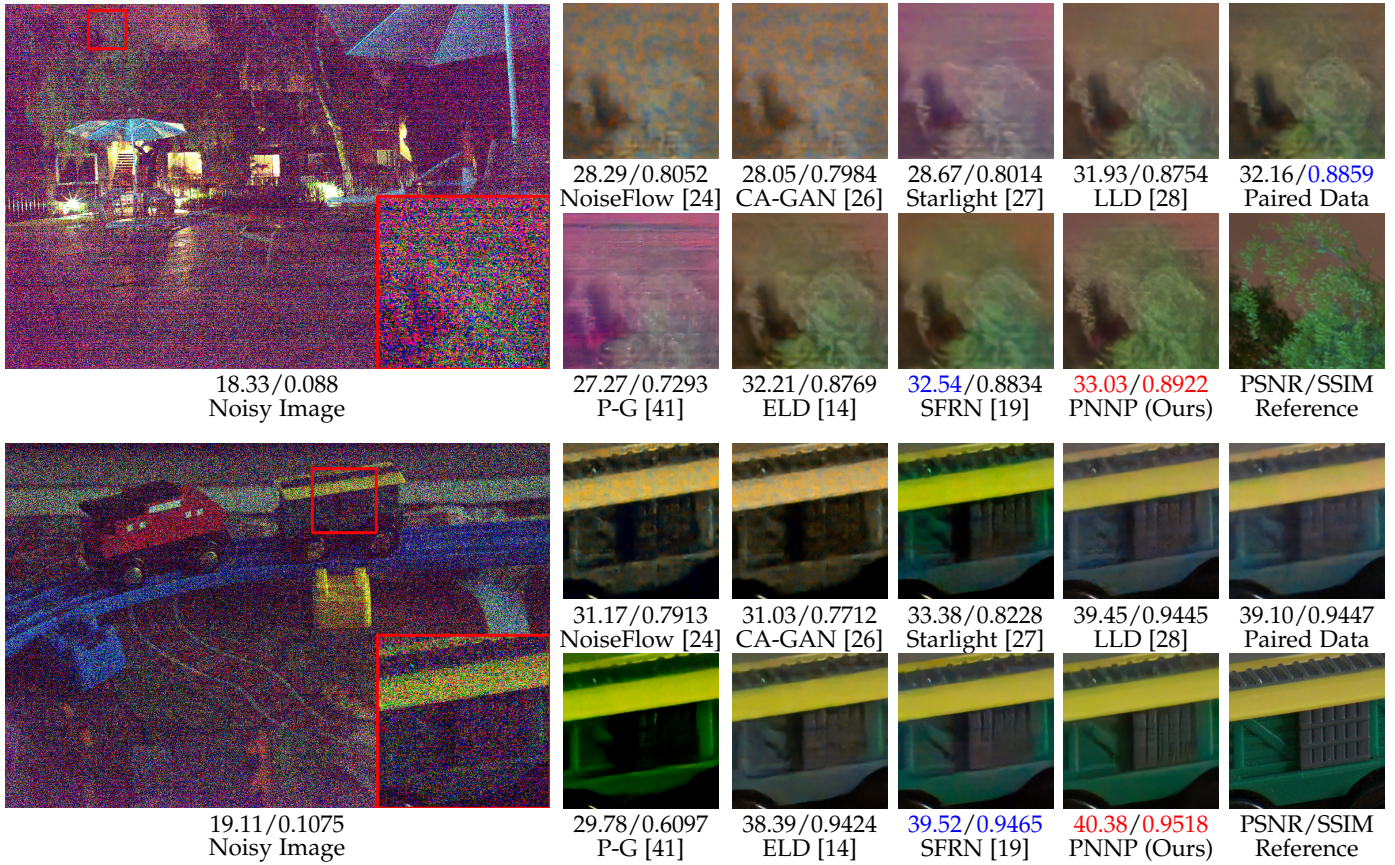


Fig. 6. Raw image denoising results on images from the SID dataset. The red color indicates the best results and the blue color indicates the second-best results. (Best viewed with zoom-in)

data coming from different data formation models. Fig. 5 and Fig. 6 have shown the comparisons on ELD dataset and SID dataset, respectively.

The model trained with synthetic data based on physics-based noise models exhibits limited effectiveness in removing real-world noise. In low-light scenarios, the synthetic data generated by the P-G [41] lacks authenticity due to significant deviations from the real noise model. As a result, denoising results exhibit noticeable color bias and stripe artifacts. While the ELD [14] enhances the modeling of read noise upon the P-G, it still falls short compared to the real noise model. The absence of fixed-pattern noise modeling in the ELD leads to prominent pattern noise in denoising results and a failure to restore fine textures. In the case of the SFRN [19], which synthesizes data by sampling real read noise, the complexity of real noise poses challenges for the network to learn accurate data mappings. Therefore, persistent fixed-pattern noise remains in denoising results, indicating the potential for further improvement in restoring fine textures. Learning from paired real data, which incorporates multiple types of noise, often yields blurry denoising results and poses difficulties in achieving model generalization.

Learning-based noise modeling methods face challenges in ensuring the accuracy of the learned noise model. While Noise Flow [24] is effective in certain scenarios, its limitations in representational ability pose challenges in capturing complex pattern noise. As a consequence, we can

obviously observe color bias and blurriness in denoising results obtained with Noise Flow. Similarly, the unstable supervision approach employed by CA-GAN [26] leads to a noise model that closely resembles the initial model in terms of representational ability. Therefore, the denoising results obtained from CA-GAN also perform obvious color bias and blurriness. Both Starlight [27] and LLD [28] employ neural noise modeling by learning noise model parameters. However, Starlight suffers from limited accuracy in its physical priors and an unreasonable network structure, leading to significant color bias in the denoising results. While LLD improves noise decomposition and simplifies data complexity, the inadequacy of its supervision approach still hinders the restoration of texture details in denoising results.

In contrast, our method achieves the most exact color and clearest textures in the majority of scenarios in public datasets. Benefiting from accurate noise neural proxies, the corresponding denoising results are exempt from obvious residual noise and effectively remove various complex noises including fixed-pattern noise.

### 4.3 Ablation Study

We conduct ablation studies from both the perspectives of noise modeling and image denoising to evaluate the effectiveness of our proposed contributions: PND, PPM, and DDL. The quantitative results of the ablation studies are shown in Table 2. We visualize representative comparison

TABLE 2

Ablation study of different modules we proposed on noise modeling and low-light raw image denoising. The underline indicates the best results.

Method	Condition	Noise Modeling		Image Denoising	
		Pixel-wise Noise KLD↓ / R <sup>2</sup> ↑	Dark Frame Noise KLD↓ / R <sup>2</sup> ↑	ELD [14] PSNR↑ / SSIM↑	SID [12] PSNR↑ / SSIM↑
PND	w/ Gaussian	0.0073 / 0.9682	0.0246 / 0.9601	40.12 / 0.8274	37.05 / 0.8255
	w/ ELD	0.0134 / 0.9837	0.0257 / 0.9685	44.44 / 0.9649	39.05 / 0.9303
	w/o Noise Decoupling	0.0300 / 0.9986	0.3135 / 0.9509	42.49 / 0.9377	36.75 / 0.8772
	PNNP (Ours)	<u>0.0021</u> / <u>0.9997</u>	<u>0.0201</u> / <u>0.9789</u>	<u>45.95</u> / <u>0.9739</u>	<u>40.75</u> / <u>0.9424</u>
PPM	w/o 1×1 Conv	0.0023 / <u>0.9997</u>	<u>0.0201</u> / <u>0.9789</u>	45.01 / 0.9669	39.68 / 0.9213
	w/o Dual Branch	0.0050 / 0.9961	0.0230 / 0.9731	45.89 / 0.9727	40.55 / 0.9388
	PNNP (Ours)	<u>0.0021</u> / <u>0.9997</u>	<u>0.0201</u> / <u>0.9789</u>	<u>45.95</u> / <u>0.9739</u>	<u>40.75</u> / <u>0.9424</u>
DDL	w/o $L_{quantile}$	0.0032 / 0.9740	0.0223 / 0.9629	45.62 / 0.9711	40.47 / 0.9366
	w/o $L_{CDF}$	0.0024 / 0.9995	0.0206 / 0.9788	45.79 / 0.9724	40.61 / 0.9398
	w/o Random Sampling	0.0241 / 0.9996	0.0205 / 0.9784	45.77 / 0.9726	40.59 / 0.9392
	PNNP (Ours)	<u>0.0021</u> / <u>0.9997</u>	<u>0.0201</u> / <u>0.9789</u>	<u>45.95</u> / <u>0.9739</u>	<u>40.75</u> / <u>0.9424</u>

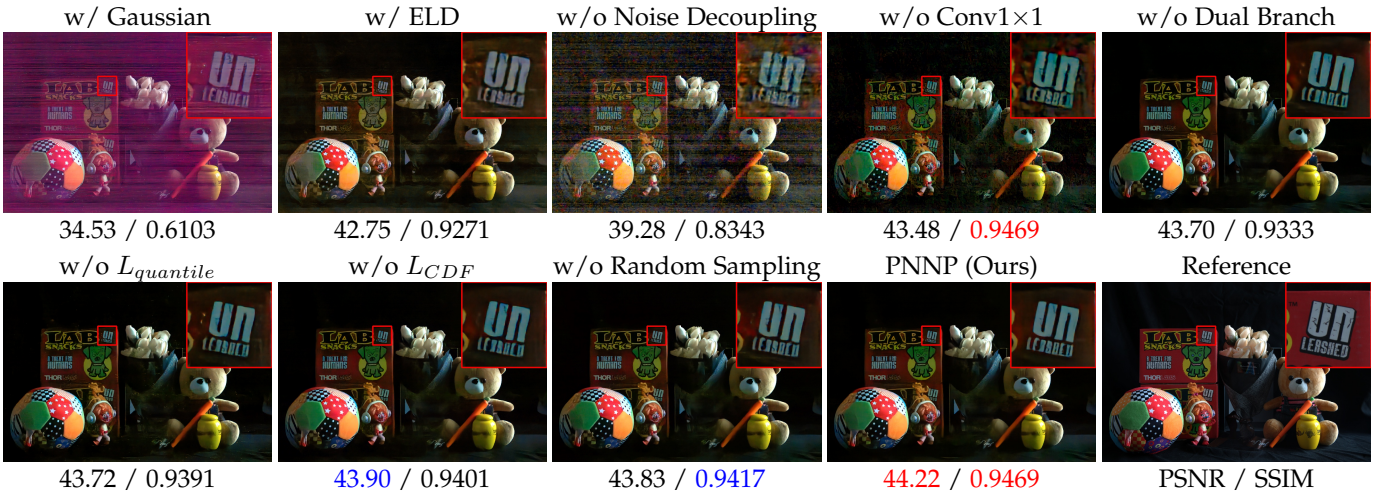


Fig. 7. A representative visual comparison of ablation studies on the ELD dataset. The red color indicates the best results and the blue color indicates the second-best results. (Best viewed with zoom-in)

of ablation studies at ISO-1600 in Fig. 7 and Fig. 8. All the ablation studies are performed on the SonyA7S2 camera.

To evaluate the performance of noise modeling, we employ the KL divergence (KLD) and coefficient of determination ( $R^2$ ) as evaluation metrics on real noise [53]. Two types of real noise are used: pixel-wise noise and dark frame noise. Pixel-wise noise represents the high-bit pixel-wise noise decoupled by PND, which serves as the ground truth during training. Dark frame noise refers to the original dark frame without PND, which serves as the noise modeling target for our PNNP framework. The calculation process of KLD and  $R^2$  is kept pace with the approaches described in Noise Flow [24] and ELD [13], [14], respectively.

To evaluate the performance of image denoising, we employed the PSNR and the SSIM on the public datasets. Since the evaluation metrics used for noise modeling cannot fully capture all the characteristics of the noise model, we consider the denoising performance corresponding to the noise model as the most crucial evaluation metric.

### 4.3.1 Ablation on PND

PND plays a vital role in bridging between physics-based noise modeling and learning-based noise modeling.

To demonstrate its effectiveness, we select two classical physics-based noise modeling methods (Gaussian and ELD) as baselines and also explore the case of direct learning without noise decoupling. As shown in Table 2, compared to the classical physics-based noise modeling, we achieved substantial improvements in the noise model. The performance of directly learning the noise model without noise decoupling is even inferior to that of the classical physics-based noise modeling, indicating that PND is indispensable for the PNNP framework.

### 4.3.2 Ablation on PPM

We study the effectiveness of the two Physics-guided module designs proposed by PPM in Table 2.

Our first design is using  $1 \times 1$  convolutions instead of  $3 \times 3$  convolutions to preserve the spatially independent prior of pixel-wise noise. In the ablation study, we replace all  $1 \times 1$  convolutions with  $3 \times 3$  convolutions. While the evaluation metrics for noise modeling may seem promising, the denoising results obtained using this noise model exhibit noticeable residual pattern noise, as shown in Fig. 7. In the absence of explicitly considering spatially correlated noise

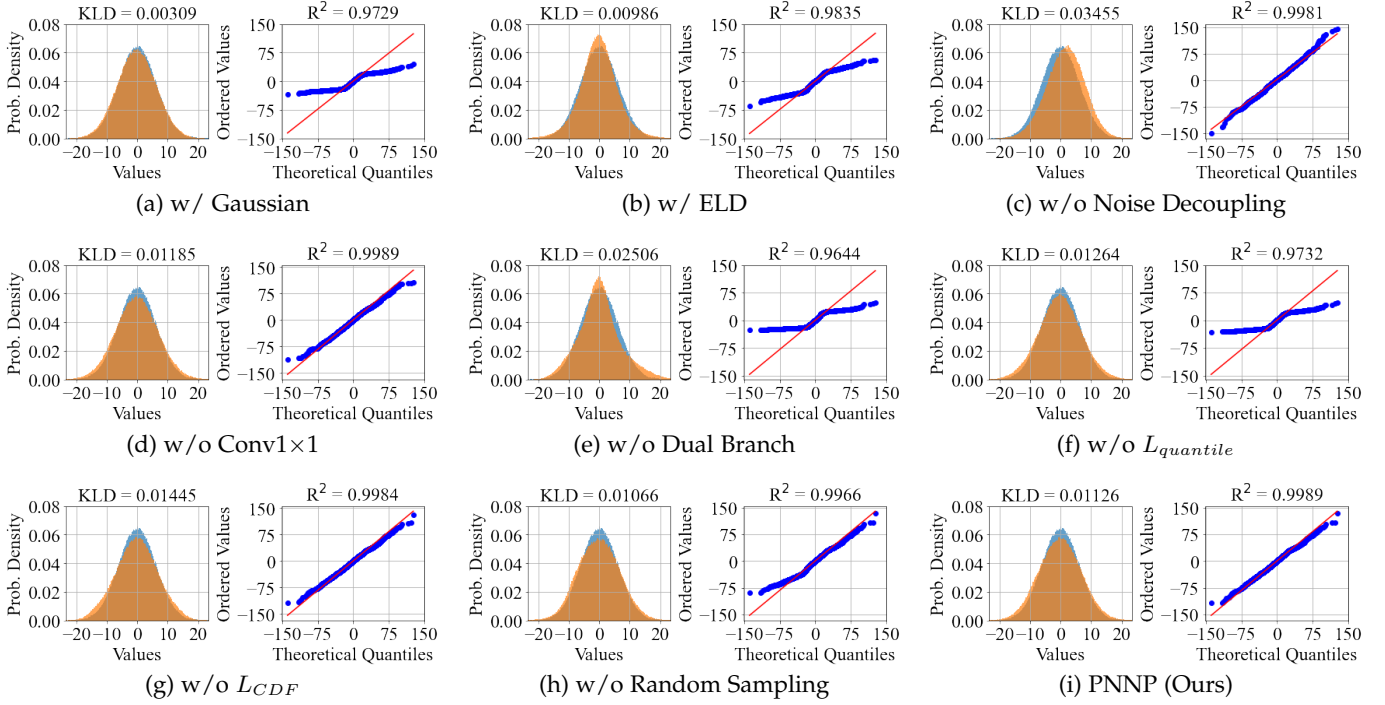


Fig. 8. A distribution comparison of ablation studies on pixel-wise noise at ISO-1600. Each subfigure consists of two parts: the left part shows a comparison of the probability density functions, while the right part shows the probability plot. The blue histogram represents the distribution of real pixel-wise noise, while the orange histogram represents the distribution of synthetic noise. The red line represents the quantiles of the real noise distribution, and the blue points represent the quantiles of the synthetic noise distribution.

components, the network spontaneously learns to exploit neighborhood information to optimize the noise model, inadvertently introducing spatial correlation. The unacceptable pattern noise highlights the significance of our pixel-wise independent module design.

Our second design is the network structure based on the sensor imaging mechanisms. In the ablation study, we change the ISO-aware dual-branch structure to a single branch. Without the physics-guided network structure design, the noise proxy model not only loses the physical interpretability but also exhibits a noticeable decrease in the accuracy of noise modeling, which highlights the importance of our ISO-aware dual-branch design.

### 4.3.3 Ablation on DDL

DDL can be briefly divided into three components: quantile loss, CDF loss, and random sampling strategy. We conducted an ablation study on each of these components, as shown in Table 2.

The quantile loss focuses on supervising the long-tail region of the noise distribution, which is consistent with the emphasis of  $R^2$ . Without quantile loss, the ability of the neural proxy framework to model the long-tail distribution significantly decreases. It is reflected in the degradation of evaluation metrics in noise modeling and the appearance of artifacts resembling bad pixels in denoised images, as shown in Fig. 8. The CDF loss focuses on supervising the central region of the noise distribution, which is the same as the emphasis of KLD. Without CDF loss, the modeling accuracy of the proxy model slightly decreases, resulting in a slight decrease in evaluation metrics. The random sampling strategy provides sufficient supervision for proxy model

training. Without the random sampling strategy, the proxy model struggles to converge stably, resulting in a decrease in evaluation metrics. The complete DDL consistently provides reliable and stable supervision for PPM, contributing to the best performance in both noise modeling and corresponding image denoising results.

## 4.4 Denoising on Real Imaging Scenarios

Lastly, the generalizability of our method is evaluated on real-world imaging scenarios. Our experiments are conducted on a low-light denoising dataset captured using the Redmi K30, a mobile phone equipped with an IMX686 sensor. All noisy images are captured at the maximum analog gain corresponding to ISO-6400, with an additional  $4\times$  digital gain applied. Fig. 9 shows the comparisons conducted on some representative real imaging scenarios. The results obtained are consistent with our comparative experiments on public datasets. Notably, our method consistently achieves the best denoising results, preserving clear textures and exact colors. These findings demonstrate the high generalizability of our method.

## 5 DISCUSSION

### 5.1 Data for Noise Modeling

One important premise often overlooked in noise modeling research is that real data is always essential in practical noise modeling. Learning-based approaches rely on real data to train noise models, while physics-based methods utilize real data for calibrating noise parameters. Although noise modeling methods are generally applicable, the model parameters exhibit sensor-specific characteristics. Hence, a robust

Input	Paired Data	P-G [41]	ELD [14]	SFRN [19]	PNNP (Ours)	Reference
25.82 / 0.2597	45.49 / 0.9806	44.37 / 0.9721	45.27 / 0.9765	45.75 / 0.9810	46.19 / 0.9839	PSNR / SSIM
23.56 / 0.2314	44.65 / 0.9864	41.42 / 0.9756	44.16 / 0.9848	44.32 / 0.9860	45.02 / 0.9890	PSNR / SSIM
24.40 / 0.2593	40.88 / 0.9631	39.14 / 0.9506	40.49 / 0.9544	40.75 / 0.9625	41.05 / 0.9638	PSNR / SSIM
25.55 / 0.2505	44.73 / 0.9749	42.76 / 0.9468	41.19 / 0.9155	42.47 / 0.9367	45.12 / 0.9783	PSNR / SSIM

Fig. 9. Raw image denoising results on low-light images captured by a Redmi K30 camera. The red color indicates the best results and the blue color indicates the second-best results. (Best viewed with zoom-in)

and practical noise modeling approach should address the inherent challenges associated with real data quality.

The quality of real data directly influences the quality of the resulting noise model. The overlook for data is particularly severe in learning-based noise modeling methods. The existing paradigm of learning-based noise modeling, which involves learning the clean-to-noise mapping from paired real data, has several issues from a data perspective. This paradigm relies on large-scale high-quality paired real data, which is often challenging to obtain. On one side, underdeveloped data acquisition protocol often results in signal misalignment within the paired real data. On the other side, the coupling of excessive noise models within the paired real data makes it challenging for neural networks to accurately approximate the real noise model. In summary, data defects hinder the performance of the existing learning-based noise modeling paradigm in practical scenarios.

Compare to learning-based noise modeling, physics-based noise modeling relies on real data collected by cameras specifically for calibration purposes, such as flat-field frames for calibrating signal-dependent noise and dark frames for calibrating signal-independent noise. The calibration process is independent of paired real data, eliminating signal misalignment. From a data perspective, the data required for physics-based noise modeling is easier to obtain and of higher quality compared to learning-based noise modeling.

Based on these insights, we propose a new paradigm for noise modeling that focuses on learning the noise model from calibration data (dark frames) instead of paired real data. The data-centric perspective serves as the driving force behind our analysis and problem-solving approach.

## 5.2 Distribution Measurement Matters

The measurement of the distance between two noise distributions poses a challenge, which is the primary obstacle for learning-based noise modeling methods to accurately represent real noise. In Section 3.4, we discussed the issue of distribution measurement metrics during proxy model training. In practical evaluation scenarios, this problem becomes even more difficult. Similar to other generative tasks, there is currently no perfect solution for directly measuring the distance between non-i.i.d. noise in noise modeling. The KLD and  $R^2$  used in the ablation study of this paper also fail to account for spatially correlated factors, leading to anomalous noise modeling evaluation metrics without  $1 \times 1$  convolution in Section 4.3.2.

We acknowledge that evaluating noise modeling on complete real noise, which includes signal-dependent noise, would be the ideal approach, but reliable evaluation metrics for this purpose are currently lacking. Considering the presence of signal misalignment even in paired real data, we believe that the existing direct evaluation metrics for noise modeling hold limited reference value. Therefore, based on these considerations, we give up to directly compare the noise modeling metrics of all methods on the public datasets.

It is important to highlight that our distribution measurement in noise modeling is unique. Unlike other learning-based noise modeling methods that commonly employ indirect measurement techniques, we take a different approach. Previous methods transform the unknown noise distribution to a known distribution (e.g., Gaussian distribution) through differentiable operations, then measure the distributions to supervise the training process. However,

TABLE 3

Quantitative results (PSNR/SSIM) of different methods on SonyA7S2 Camera (ELD dataset and SID dataset). “\*” donate the method trained with paired real data. The red color indicates the best results and the blue color indicates the second-best results.

Method	ELD [14]	SID [12]
	PSNR / SSIM	PSNR / SSIM
ELD [14]	44.44 / 0.9649	39.05 / 0.9303
PMN [42]	45.51 / 0.9780	40.42 / 0.9461
LLD [28]	44.93 / 0.9712	39.56 / 0.9348
LLD* [28]	45.85 / <b>0.9814</b>	40.52 / <b>0.9472</b>
PNNP (Ours)	<b>46.00</b> / 0.9735	<b>40.75</b> / 0.9409
PNNP* (Ours)	<b>46.13</b> / <b>0.9820</b>	<b>40.77</b> / <b>0.9480</b>

in these indirect measurement methods, the reliability of the neural network as part of the measurement function is questionable. In contrast, our framework starts from the data perspective and directly decouples non-i.i.d. noise into measurable components through physics-guided noise decoupling. Instead of forcing complex data to fit measurement methods, we simplify the data to align with reliable measurement techniques. This comprehensive consideration of noise distribution measurement is another fundamental reasons for our excellent denoising performance.

### 5.3 Paired Real Data Meets Noise Modeling

PMN [42] introduces a novel strategy that combines paired real data and noise modeling, forming a kind of augmented hybrid data. As PMN encompasses more than just noise modeling, we exclude it from the comparison in Section 4.2.

Recently, LLD [28] proposed a hybrid training strategy based on PMN, comprising two strategies: the dark shading correction strategy and the zero-mean noise strategy. The dark shading correction strategy relies on paired real data, while the zero-mean noise strategy relies on data synthesized based on noise modeling. By integrating the read noise model of LLD via the zero-mean noise strategy, LLD\* achieves competitive performance in low-light denoising. The hybrid training strategy provides a fair approach for comparison with augmented hybrid data. We incorporate our method into this hybrid training strategy, denoted as PNNP\*. We compare our method with existing hybrid data-based methods and corresponding noise modeling methods, as shown in Table 3. After applying the hybrid training strategy, PNNP\* achieves state-of-the-art quantitative results, effectively and robustly suppressing complex pattern noise. The comparison further supports the superiority of our PNNP framework.

## 6 CONCLUSION

In this paper, we propose a novel strategy for noise modeling, which involves learning noise neural proxy from dark frames instead of paired real data. Based on the new strategy, we introduce a physics-guided noise neural proxy framework. Our framework leverages the physical priors of the sensor to decouple the complex noise, constrain the optimization process, and provide reliable supervision, thereby

further improving the performance of noise neural proxy. Firstly, we propose a physics-guided noise decoupling strategy to handle different levels of noise in a flexible manner. Secondly, we propose a physics-guided proxy model incorporating physical priors to constrain the generated noise. Finally, we propose a differentiable distribution-oriented loss function to efficiently supervise the random noise variables. By combining statistical constraints based on physical priors with the learning capabilities of neural proxies, our framework enables the continuous representation of real sensor noise. Experimental results on public datasets and real-world imaging scenarios demonstrate the competitive performance of our denoising model based on the proposed PNNP framework, highlighting its effectiveness in noise modeling.

## REFERENCES

- [1] K. Zhang, W. Zuo, Y. Chen, D. Meng, and L. Zhang, “Beyond a gaussian denoiser: Residual learning of deep cnn for image denoising,” *IEEE Transactions on Image Processing (TIP)*, vol. 26, pp. 3142–3155, 2017.
- [2] K. Zhang, W. Zuo, and L. Zhang, “Ffdnet: Toward a fast and flexible solution for cnn-based image denoising,” *IEEE Transactions on Image Processing (TIP)*, vol. 27, no. 9, pp. 4608–4622, 2018.
- [3] S. Guo, Z. Yan, K. Zhang, W. Zuo, and L. Zhang, “Toward convolutional blind denoising of real photographs,” in *IEEE/CVF Conference on Computer Vision and Pattern Recognition (CVPR)*, 2019, pp. 1712–1722.
- [4] Z. Yue, H. Yong, Q. Zhao, D. Meng, and L. Zhang, “Variational denoising network: Toward blind noise modeling and removal,” *Advances in Neural Information Processing Systems (NeurIPS)*, vol. 32, 2019.
- [5] S. W. Zamir, A. Arora, S. Khan, M. Hayat, F. S. Khan, M.-H. Yang, and L. Shao, “Multi-stage progressive image restoration,” in *IEEE/CVF Conference on Computer Vision and Pattern Recognition (CVPR)*, 2021, pp. 14 821–14 831.
- [6] S. Cheng, Y. Wang, H. Huang, D. Liu, H. Fan, and S. Liu, “Nbnnet: Noise basis learning for image denoising with subspace projection,” in *IEEE/CVF Conference on Computer Vision and Pattern Recognition (CVPR)*, 2021, pp. 4896–4906.
- [7] Z. Tu, H. Talebi, H. Zhang, F. Yang, P. Milanfar, A. Bovik, and Y. Li, “Maxim: Multi-axis mlp for image processing,” in *IEEE/CVF Conference on Computer Vision and Pattern Recognition (CVPR)*, 2022, pp. 5769–5780.
- [8] L. Chen, X. Lu, J. Zhang, X. Chu, and C. Chen, “Hinet: Half instance normalization network for image restoration,” in *IEEE/CVF Conference on Computer Vision and Pattern Recognition (CVPR)*, 2021, pp. 182–192.
- [9] S. W. Zamir, A. Arora, S. Khan, M. Hayat, F. S. Khan, and M.-H. Yang, “Restormer: Efficient transformer for high-resolution image restoration,” in *IEEE/CVF Conference on Computer Vision and Pattern Recognition (CVPR)*, 2022, pp. 5728–5739.
- [10] T. Plötz and S. Roth, “Benchmarking denoising algorithms with real photographs,” in *IEEE/CVF Conference on Computer Vision and Pattern Recognition (CVPR)*, 2017, pp. 2750–2759.
- [11] A. Abdelhamed, S. Lin, and M. S. Brown, “A high-quality denoising dataset for smartphone cameras,” in *IEEE/CVF Conference on Computer Vision and Pattern Recognition (CVPR)*, 2018, pp. 1692–1700.
- [12] C. Chen, Q. Chen, J. Xu, and V. Koltun, “Learning to see in the dark,” in *IEEE/CVF Conference on Computer Vision and Pattern Recognition (CVPR)*, 2018, pp. 3291–3300.
- [13] K. Wei, Y. Fu, J. Yang, and H. Huang, “A physics-based noise formation model for extreme low-light raw denoising,” in *IEEE/CVF Conference on Computer Vision and Pattern Recognition (CVPR)*, 2020, pp. 2755–2764.
- [14] K. Wei, Y. Fu, Y. Zheng, and J. Yang, “Physics-based noise modeling for extreme low-light photography,” *IEEE Transactions on Pattern Analysis and Machine Intelligence (TPAMI)*, pp. 1–18, 2021.
- [15] B. Zhang, Y. Guo, R. Yang, Z. Zhang, J. Xie, J. Suo, and Q. Dai, “Darkvision: A benchmark for low-light image/video perception,” *arXiv preprint arXiv:2301.06269*, 2023.

- [16] H. Yue, C. Cao, L. Liao, and J. Yang, "Rvideformer: Efficient raw video denoising transformer with a larger benchmark dataset," *arXiv preprint arXiv:2305.00767*, 2023.
- [17] T. Brooks, B. Mildenhall, T. Xue, J. Chen, D. Sharlet, and J. T. Barron, "Unprocessing images for learned raw denoising," in *IEEE/CVF Conference on Computer Vision and Pattern Recognition (CVPR)*, 2019, pp. 11 036–11 045.
- [18] Y. Wang, H. Huang, Q. Xu, J. Liu, Y. Liu, and J. Wang, "Practical deep raw image denoising on mobile devices," in *European Conference on Computer Vision (ECCV)*, 2020, pp. 1–16.
- [19] Y. Zhang, H. Qin, X. Wang, and H. Li, "Rethinking noise synthesis and modeling in raw denoising," in *IEEE/CVF International Conference on Computer Vision (ICCV)*, 2021, pp. 4573–4581.
- [20] B. Jähne, "Emva 1288 standard for machine vision: Objective specification of vital camera data," *Optik & Photonik*, vol. 5, no. 1, pp. 53–54, 2010.
- [21] G. C. Holst and T. S. Lomheim, *CMOS/CCD Sensors and Camera Systems, Second Edition*. SPIE, 2011.
- [22] R. Gow, D. Renshaw, K. Findlater, L. A. Grant, S. Mcleod, J. Hart, and R. Nicol, "A comprehensive tool for modeling cmos image-sensor-noise performance," *IEEE Transactions on Electron Devices (TED)*, vol. 54, pp. 1321–1329, 2007.
- [23] M. Konnik and J. Welsh, "High-level numerical simulations of noise in ccd and cmos photosensors: Review and tutorial," *arXiv preprint arXiv:1412.4031*, pp. 1–21, 2014.
- [24] A. Abdelhamed, M. A. Brubaker, and M. S. Brown, "Noise flow: Noise modeling with conditional normalizing flows," in *IEEE/CVF International Conference on Computer Vision (ICCV)*, 2019, pp. 3165–3173.
- [25] Z. Yue, Q. Zhao, L. Zhang, and D. Meng, "Dual adversarial network: Toward real-world noise removal and noise generation," in *European Conference on Computer Vision (ECCV)*, 2020, pp. 41–58.
- [26] K.-C. Chang, R. Wang, H.-J. Lin, Y.-L. Liu, C.-P. Chen, Y.-L. Chang, and H.-T. Chen, "Learning camera-aware noise models," in *European Conference on Computer Vision (ECCV)*, 2020, pp. 343–358.
- [27] K. Monakhova, S. R. Richter, L. Waller, and V. Koltun, "Dancing under the stars: Video denoising in starlight," in *IEEE/CVF Conference on Computer Vision and Pattern Recognition (CVPR)*, 2022, pp. 16 241–16 251.
- [28] Y. Cao, M. Liu, S. Liu, X. Wang, L. Lei, and W. Zuo, "Physics-guided iso-dependent sensor noise modeling for extreme low-light photography," in *IEEE/CVF Conference on Computer Vision and Pattern Recognition (CVPR)*, 2023, pp. 5744–5753.
- [29] I. S. McLean, *Electronic Imaging in Astronomy: Detectors and Instrumentation*. Springer Science & Business Media, 2008.
- [30] M. S. Joens, C. Huynh, J. M. Kasuboski, D. Ferranti, Y. J. Sigal, F. Zeitvogel, M. Obst, C. J. Burkhardt, K. P. Curran, S. H. Chalasani et al., "Helium ion microscopy (him) for the imaging of biological samples at sub-nanometer resolution," *Scientific reports*, vol. 3, no. 1, pp. 1–7, 2013.
- [31] S. W. Hasinoff, D. Sharlet, R. Geiss, A. Adams, J. T. Barron, F. Kainz, J. Chen, and M. Levoy, "Burst photography for high dynamic range and low-light imaging on mobile cameras," *ACM Transactions on Graphics (TOG)*, vol. 35, no. 6, pp. 1–12, 2016.
- [32] M. Aharon, M. Elad, and A. Bruckstein, "K-svd: An algorithm for designing overcomplete dictionaries for sparse representation," *IEEE Transactions on Signal Processing (TSP)*, vol. 54, no. 11, pp. 4311–4322, 2006.
- [33] M. Elad and M. Aharon, "Image denoising via sparse and redundant representations over learned dictionaries," *IEEE Transactions on Image Processing (TIP)*, vol. 15, no. 12, pp. 3736–3745, 2006.
- [34] S. Gu, L. Zhang, W. Zuo, and X. Feng, "Weighted nuclear norm minimization with application to image denoising," in *IEEE/CVF Conference on Computer Vision and Pattern Recognition (CVPR)*, 2014, pp. 2862–2869.
- [35] A. Buades, B. Coll, and J.-M. Morel, "A non-local algorithm for image denoising," in *IEEE/CVF Conference on Computer Vision and Pattern Recognition (CVPR)*, 2005, pp. 60–65.
- [36] K. Dabov, A. Foi, V. Katkovnik, and K. Egiazarian, "Image denoising by sparse 3-d transform-domain collaborative filtering," *IEEE Transactions on Image Processing (TIP)*, vol. 16, pp. 2080–2095, 2007.
- [37] J. Portilla, V. Strela, M. J. Wainwright, and E. P. Simoncelli, "Image denoising using scale mixtures of gaussians in the wavelet domain," *IEEE Transactions on Image Processing (TIP)*, vol. 12, no. 11, pp. 1338–1351, 2003.
- [38] L. I. Rudin, S. Osher, and E. Fatemi, "Nonlinear total variation based noise removal algorithms," *Physica D: nonlinear phenomena*, vol. 60, no. 14, pp. 259–268, 1992.
- [39] C. Chen, Q. Chen, M. N. Do, and V. Koltun, "Seeing motion in the dark," in *IEEE/CVF International Conference on Computer Vision (ICCV)*, 2019, pp. 3185–3194.
- [40] C. Li, C. Guo, L.-H. Han, J. Jiang, M.-M. Cheng, J. Gu, and C. C. Loy, "Low-light image and video enhancement using deep learning: A survey," *IEEE Transactions on Pattern Analysis and Machine Intelligence (TPAMI)*, pp. 1–19, 2021.
- [41] A. Foi, M. Trimeche, V. Katkovnik, and K. Egiazarian, "Practical poissonian-gaussian noise modeling and fitting for single-image raw-data," *IEEE Transactions on Image Processing (TIP)*, vol. 17, no. 10, pp. 1737–1754, 2008.
- [42] H. Feng, L. Wang, Y. Wang, and H. Huang, "Learnability enhancement for low-light raw denoising: Where paired real data meets noise modeling," in *Proceedings of the 30th ACM International Conference on Multimedia (ACMMM)*, 2022, pp. 1436–1444.
- [43] G. E. Healey and R. Kondepudy, "Radiometric ccd camera calibration and noise estimation," *IEEE Transactions on Pattern Analysis and Machine Intelligence (TPAMI)*, vol. 16, no. 3, pp. 267–276, 1994.
- [44] M. Makitalo and A. Foi, "A closed-form approximation of the exact unbiased inverse of the anscombe variance-stabilizing transformation," *IEEE Transactions on Image Processing (TIP)*, vol. 20, no. 9, pp. 2697–2698, 2011.
- [45] —, "Optimal inversion of the generalized anscombe transformation for poisson-gaussian noise," *IEEE Transactions on Image Processing (TIP)*, vol. 22, no. 1, pp. 91–103, 2013.
- [46] D. Li, Y. Zhang, K. L. Law, X. Wang, H. Qin, and H. Li, "Efficient burst raw denoising with variance stabilization and multi-frequency denoising network," *International Journal of Computer Vision (IJCV)*, vol. 130, no. 8, pp. 2060–2080, 2022.
- [47] H. Wach and E. R. Dowski Jr, "Noise modeling for design and simulation of computational imaging systems," in *Visual Information Processing*, 2004, pp. 159–170.
- [48] L. Song and H. Huang, "Fixed pattern noise removal based on a semi-calibration method," *IEEE Transactions on Pattern Analysis and Machine Intelligence (TPAMI)*, pp. 1–14, 2023.
- [49] J. Nakamura, *Image Sensors and Signal Processing for Digital Still Cameras*. CRC press, 2017.
- [50] L. D. Tran, S. M. Nguyen, and M. Arai, "Gan-based noise model for denoising real images," in *Proceedings of the Asian Conference on Computer Vision (ACCV)*, 2020.
- [51] J. Wang, Y. Yu, S. Wu, C. Lei, and K. Xu, "Rethinking noise modeling in extreme low-light environments," in *IEEE International Conference on Multimedia and Expo (ICME)*, 2021, pp. 1–6.
- [52] M. Maggioni, E. Sánchez-Monge, and A. Foi, "Joint removal of random and fixed-pattern noise through spatiotemporal video filtering," *IEEE Transactions on Image Processing (TIP)*, vol. 23, no. 10, pp. 4282–4296, 2014.
- [53] E. C. Morgan, M. Lackner, R. M. Vogel, and L. G. Baise, "Probability distributions for offshore wind speeds," *Energy Conversion and Management*, vol. 52, no. 1, pp. 15–26, 2011.
- [54] I. Goodfellow, J. Pouget-Abadie, M. Mirza, B. Xu, D. Warde-Farley, S. Ozair, and Y. Bengio, "Generative adversarial networks, 1–9," vol. 27, 2014, pp. 1–9.
- [55] D. P. Kingma and P. Dhariwal, "Glow: Generative flow with invertible 1x1 convolutions," in *Advances in Neural Information Processing Systems*, S. Bengio, H. Wallach, H. Larochelle, K. Grauman, N. Cesa-Bianchi, and R. Garnett, Eds., vol. 31, 2018, pp. 1–10.
- [56] D. P. Kingma and J. Ba, "Adam: A method for stochastic optimization," in *International Conference on Learning Representations (ICLR)*, 2015, pp. 1–15.
- [57] I. Loshchilov and F. Hutter, "SGDR: stochastic gradient descent with warm restarts," in *International Conference on Learning Representations (ICLR)*, 2017, pp. 1–16.
- [58] O. Ronneberger, P. Fischer, and T. Brox, "U-net: Convolutional networks for biomedical image segmentation," in *Medical Image Computing and Computer-Assisted Intervention (MICCAI)*, 2015, pp. 234–241.



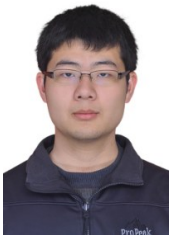
**Hansen Feng** received the BS degree from the University of Science and Technology Beijing, China, in 2020. He is currently a Ph.D. student with the School of Computer Science and Technology, Beijing Institute of Technology. His research interests include computational photography and image processing. He received the Best Paper Runner-Up Award of ACM MM 2022.



**Lizhi Wang** (M'17) received the B.S. and Ph.D. degrees from Xidian University, Xi'an, China, in 2011 and 2016, respectively. He is currently an Associate Professor with the School of Computer Science and Technology, Beijing Institute of Technology. His research interests include computational photography and image processing. He received the Best Paper Award of IEEE VCIP 2016.



**Yiqi Huang** received the B.S. degree from the school of Information Science and Engineering, Lanzhou University, Lanzhou, China, in 2022. He is currently a M.D. student with the School of Computer Science and Technology, Beijing Institute of Technology. His research interests include computational photography and image processing.



**Yuzhi Wang** received the B.S. degree from the School of Telecommunication Engineering, Xidian University, Xi'an, China, in 2012. He received the Ph.D. degree with the Department of Electronic Engineering, Tsinghua University, Beijing, China, under the supervision of Prof. H. Yang. His research interests include wireless sensor networks, computational photography, machine learning, and deep neural networks



**Hua Huang** (SM'19) received the B.S. and Ph.D. degrees from Xi'an Jiaotong University, in 1996 and 2006, respectively. He is currently a professor in the School of Artificial Intelligence, Beijing Normal University. He is also an adjunct professor at Xi'an Jiaotong University and Beijing Institute of Technology. His main research interests include image and video processing, computational photography, and computer graphics. He received the Best Paper Award of ICML2020 / EURASIP2020 / PRCV2019 / ChinaMM2017.